Precise Shape Prediction of Human Heart Left Ventricle during Diastole Using Fluid-Solid Simulation

Arman Zohrabi, Mohammad Mehdi Alishahi*, Marzieh Alishahi

School of Mechanical Engineering, Shiraz University, Shiraz, 71936-16548,I.R. of Iran

Abstract. Using Fluid-Solid Interactions (FSI), this study presents the proper configuration and boundary conditions (BC) for precise prediction of shape and cardiac performance of human heart during diastole. The judgment is based upon comparison of deformations and volume change of left ventricle plus atrium with CT scan images for a healthy person. Usage of correct BC for left ventricle plus atrium provides more accurate results, in terms of volume of left ventricle variations compared to real values and differences are less than 1.3%. Also, shape change of ventricle compares well with scanned images.

Three different configurations are constructed from CT images as initial geometries: model A; left ventricle with thick ventricular wall and mitral valve, as an example of hypertrophic case, model B; the original left ventricle and mitral valve from scanned images and model C, which is the model B plus the original atrium geometry. Using unsteady FSI, the difference of experimental numerical ventricle volumes is expectedly large for model A, due to hypertrophy. The difference between numerical results and experiments is 6% for model B and 1.25%, for the more complete model C. Therefore, closer agreement of model C with experiment and its feasibility for more involved cases is shown.

Keywords: CFD, Left Ventricle, Mitral valve, Diastole, Fluid-Solid Interaction.

Introduction

Cardiovascular diseases are the main reason of human fatalities and disabilities in the most countries of the world. According to World Health Organization's (WHO) report, in 2019 about 17.9 million deaths due to cardiovascular diseases was reported which is 31% of total death number in the world [1].

Recently, a lot of efforts was made to cure cardiovascular diseases and reduce the fatalities caused by them. In this regard, various engineering tools have been employed to simulate the heart function [2-10]. This enhances our understandings of the phenomena involved and may affect both cure and surgery matters in future. In 1989, Peskin et al. presented the immersed body method to simulate a very simple model of the heart ventricle as a circular cavity [11]. The Peksin method was used further by others to investigate the heart simulations [12-14]. During next years,

* Corresponding Author, Email: alisha@shirazu.ac.ir, 0713 613 3024

simplified geometries with no valves were used in order to reach a feasible simulation of heart function . In 2012, Zheng [14] and his colleagues presumed a semi prolate spheroid model for the left ventricle for healthy and patient conditions while neglecting the mitral and the aortic valves. They used immersed boundary method and modelled five stages of heart function; fast filling, diastasis, atrial systole, isovolumetric contraction and systole and studied the flow pattern for both healthy and patient conditions [14-27].

More recent investigations used both CFD methods and CT scan images in a way that the blood volume inside the heart is extracted from different phases of CT images and considered as the geometry of problem [28-36]. Afterwards, the grid is generated for the geometry in different phases of CT images and for a continuous simulation, grid is interpolated between phases. For CFD simulation of blood flow inside the ventricle, some researches considered complex methods such as large eddy simulation [37]. Moreover there are some studies that investigate the nature of heart electrical interactions [38-42].

The other important issue in heart simulation is Fluid-Solid Interaction (FSI) which considers the effects of structural deformation controlled by solid strength on the fluid flow and vice versa. If the deformation of heart tissues is small, its effect on fluid flow could be neglected. But in real life, heart walls undergo large deformations, therefore the wall effect on fluid flow is significant and cannot be neglected. The FSI simulation has been widely used in CFD calculations [18-26, 43-50]. Hirosh and his colleagues studied filling of left ventricle using FSI methods while neglecting the mitral valve [14]. Similar researches carried out by Yongguang et al. [12,19], Arefin et al. [22], Nakamura [15] and Pourmand [43] who again modelled heart diastole without modelling the mitral valve. Nordsletten and colleagues modelled a real shaped left ventricle based on the CT scan images [44]. Their simulation covered the whole heart cycle of the systole and the diastole. Nevertheless, they did not model the mitral and aortic valves. Meanwhile some researchers studied the mitral valve separately; Hao Gao et al. modelled the mitral valve based on the MRI images using FSI method [45]. In their study, the mitral valve was assumed to be completely placed in a confined region filled with the blood. The physiological pressure were excreted on the valve leaflets [45]. Milan Toma and colleagues analyzed the papillary muscle force of mitral valve during heart cycle using the FSI method [46].

As the left ventricle plays an important functional role, the researchers evolve their models by adding mitral valve to left ventricle simulation. Dahl et al. and Boyang et al. considered such a model during diastole using a simplified 2D geometry [21], [23]. Afterwards, Lau et al. performed a 3D simulation of left ventricle with a real shaped mitral valve, considering the ventricle walls as solid and FSI method was only employed for the mitral valve [20]. The more developed FSI simulations during the heart cycle were carried out by Jung Hee Seo et al. [47], Kheirandish et al. [48]. In the latter investigation, the geometry of left ventricle and mitral valve were extracted from CT scan images of a specific person. The inlet velocity boundary condition in these simulations was set using the physiological discharge of blood entering the left ventricle through the mitral valve.

Although the use of physiological velocity at inlet BC, brings about the realistic values of left ventricle volume change, but the left ventricle shape and its change during the diastole would be quite unrealistic compared to CT images. This happens due to volume change enforcement by inlet velocity BC, therefore the stress and strain field should be incorrect, as well. In the present investigation, the inlet BC is changed to pressure BC in FSI simulation of left ventricle during the diastole and it is shown that the left ventricle shape during the diastole is analogous to CT scan images. Also, considering the actual heart geometry change during diastole, it is shown that a complete simultaneous FSI simulation of ventricle, atrium and mitral valve is imperative for a realistic and sound modeling of volume and wall deformation prediction of a whole left heart.

Having a more accurate model of heart deformation as described above, other effects such as different ventricle wall thickness, as an important parameter on heart function, can be investigated with more precision. Due to high blood pressure, the left ventricular wall may thicken and leads to Left Ventricular Hypertrophy (LVH) [51]. The enlarged heart muscle loses elasticity and may result in lower cardiac output. Eventually LVH increases the risk of a heart attack and stroke [52]. Therefore, it will be noteworthy to investigate the effect of ventricular wall thickness change using the above mentioned FSI technique. The obtained results may lead to a helpful tool for prediction of the cardiac output of patients suffering from LVH if the systolic phase is also carried out afterwards.

Also various models of mitral valve together with left ventricle of healthy and a tentative LVH case and the left atrium are concurrently simulated using FSI and the results are presented and discussed.

1. Problem Definition

1-1 Physical Modeling

1-1-1 Problem Geometry

In this study, the geometry of left ventricle and left atrium are extracted from CT scan images of a healthy young male at the beginning and during diastole. The mitral valve is designed and added to the geometry according to its anatomic dimensions and shape [53]. The papillary muscles are neglected as in previous investigations [20, 21, 23, 47, 54]. Considering the anatomic shape of mitral valve, its dimensions are extracted from CT scan images. The following geometrical assumptions are also made in regenerating the mitral valve structure: (1) the inlet cross section of the valve is elliptic, (2) when the valve is completely closed, its two leaflets overlap on a curved shape (3) the anterior leaflet is shorter than the posterior one.

The simulations are carried out for three different models. The model A considers the left ventricle with mitral valve, while the ventricle wall is thicker than the original wall observed in CT images, as a simple LVH model. The model B represents the real geometry of left ventricle with mitral valve, also the ventricle wall thickness is equal to its real extracted value from CT images. The model C is the most complete and real model, including the real geometry of left ventricle with mitral valve and real shaped atrium (Fig. 1).

Since detailed dimensions of the mitral valve cannot be exactly derived from CT images, the mitral valve is reconstructed according to the anatomic considerations and the real dimensions of mitral valve obtained from CT scan images of the mentioned person. Fig. 2 shows the anatomic dimensions and final geometry of mitral valve used in the present study.

1-1-2 Materials and Models

Left ventricular tissue is completely deformable with greater deformability than elastic material. Therefore, hyperelastic material would be more appropriate material model for left ventricle wall and mitral valve. Pourmand [43] proved that third-order Ogden model [55] has an acceptable accordance with experimental results for left ventricle and mitral valve. In this study, the coefficients of third order Ogden model fit to uniaxial test results were used, [43]. This model approximates an elastic material with density of 1050 [kg/m^3], Young Modulus of 10000 [Pa] and Poisson Coefficient of 0.095.

Blood is considered as Newtonian incompressible fluid [21-23, 30] with density equal to 1060 kg/m^3 and viscosity is 0.000345 Ns/m^2.

1-2 Numerical Modeling

FSI analysis is carried out based on the Two-Way FSI algorithm of ANSYS-Multiphysics software, version 17.0. FLUENT software solves Navier-Stokes equations in fluid domain and fluid forces are imposed on solid domain via FSI boundary. ANSYS Mechanical module performs structural analysis and new displacements and velocities on the fluid domain boundaries are determined. Details of numerical modeling are presented in the following sections.

1-2-1 Governing Equations and Interface BC's

The governing equations for fluid domain are Navier-Stokes and continuity equations and we considere the flow to be laminar although this assumption may be questionable at some instances of ventricle filling. General form of these equations for a Newtonian fluid are as follows;

$$\rho\left(\frac{\partial \vec{v}}{\partial t}+\vec{c}.\nabla\vec{v}\right)=-\nabla p+\mu\nabla^2\vec{v}+\vec{f} \quad (1)$$

$$T_{ij}=\mu\left(\frac{\partial v_i}{\partial x_j}+\frac{\partial v_j}{\partial x_i}\right) \quad (2)$$

$$\nabla.\left(\vec{v}\right)=0 \quad (3)$$

Where $\vec{f}$ is the body force and $\vec{c}$ is the fluid relative velocity. T_{ij} is the elements of viscous stress tensor. At in or outflow boundaries we may define velocity or pressure as a function of time, as discussed before. At walls, boundary conditions would be zero relative velocity of normal and tangential components. Alternatively, no flow through non-permeable boundary and zero slip relative velocity for normal and tangential components. However, for a FSI study, we need extra conditions for the interface between fluid and solid. These two conditions consist of kinematical condition, equal displacement and equal normal stress tensor as dynamical condition. These two conditions guarantee that the fluid and solid domains will not detach or overlap, regarding zero thickness and mas of the interface. These conditions altogether are summarized in the following.

$$\vec{u}_f = \vec{u}_s \tag{4}$$

$$\vec{v}_f = \vec{v}_s \tag{5}$$

$$\vec{n} \,.\tau_f = \vec{n} \,.\tau_s \tag{6}$$

Where $\vec{u}$ is the displacement vector and τ is the stress tensor referring to fluid and solid indicated by subscripts f and s, respectively. Also, $\vec{n}$ is the normal vector at FSI boundary.

1-2-2 Fluid Boundary Conditions

In this research, similar boundary conditions are applied to the three different models. Fig. 3 shows the boundary conditions of the fluid domain.

For all three models, the inlet boundary condition for fluid domain is the atrial pressure which is approximated by a 6th order polynomial curve fit on the physiological pressure of left atrium. Previously, Kheirandish used velocity boundary condition at the inlet that resulted in ventricular shape change that were not compatible with CT images [48]. As it will be shown, in this study, the pressure boundary condition at the inlet eventuates to more accurate results in accordance with CT images.

For model C, the same pressure boundary condition was applied but on the atrial inlets instead of inlet of mitral valve in models A and B. Fig. 4 illustrates the 6th order polynomial curve fit for atrial physiological pressure described in Guyton and Hall's medical physiology textbook [53]. It should be noted during the diastole, blood discharge through aortic valve is zero and this valve acts as a wall. Therefore, the outlet boundary condition at aortic valve is defined as wall boundary condition.

Coefficients of 6th order polynomial shown in Fig. 4 are written in table 1.

1-2-3 Solid Boundary Conditions

Solid boundary conditions for boundaries neighboring the fluid domain is of FSI type. On the other hand, solid domain should be fixed at some specific points or surfaces, therefore the ring at the ventricular outlet at the aortic valve are fixed for all models. Besides the upper ring of mitral valve, i.e. mitral annulus, is fixed for models A and B. Moreover, for model C, the rings at atrial inlets are assumed to be fixed boundary conditions (Fig. 5).

1-2-4 Computational Grid

Three different unstructured tetrahedron grids are generated for each model to find the grid independent solution (see Fig. 6). Table 2 shows sizes of grids, i.e. number of grid elements, for both solid and fluid domains for each model.

For fluid domain grid study is performed regarding the average pressure of a sample plane at the middle of left ventricle. For solid domain, grid study is done based on the maximum of von Mises stress on the mitral valve. For all cases, after three steps of mesh refinement (see table 2), grid independent results are achieved. Furthermore, three different time steps are considered; 0.01s, 0.005s and 0.002s. For all three models after decreasing time steps as per three steps, the time step independent results are also obtained. Fig. 7 demonstrates an instance of grid and time step independency study results for fluid domain. Here, convergence of average pressure on the sample plane shows that grid and time step independent solution is achieved. It should be noted that each simulation took one to two days' time on a core-i7 eight cores system with 16GB RAM.

2. Results and Discussion

2-1 Fluid domain

2-1-1 Left ventricular volume change and pressure

As it was mentioned earlier, the main objective of current study is to present an appropriate modelling of heart during diastole and verify the numerical results with experimental data. One of the chief parameters that is used for this verification is time variation of left ventricular volume.

Fig. 8 shows results of three models; A, B, C simulations with inlet pressure BC as introduced in the previous section. Also Kheirandish's [48] results with the same initial geometry of left ventricle

but with the inlet velocity BC are added to this figure. For comparison the CT scan data are also added to Fig. 8. The CT scan image is used to calculate volume of the left ventricle generated using the Mimics software (Materialise NV, Leuven, Belgium) extracted from images in 3 directions.

In Fig. 8(b) ventricular volume change of models B and C are compared with the real values obtained from CT images. Note that initial geometry of model B and C are both uniquely set from CT images. It can be seen that the volume variation of model C is closer to the real values than the predictions of model B. Only for time interval 0.17s to 0.32s, there is a relative deviation between model C and experimental results. This figure shows that maximum and mean error of volume difference of models B and C are 15.6%, 6% and 8.5%, 1.25%, respectively. This indicates importance of considering a more geometrical complete model of heart i.e. model C instead of model B, for precise determination of volume change. We will compare the actual and simulated shapes at different times during diastole in later sections. Therefore, the improvement would be about four times, if we consider the more precise and complex geometry of Model C.

Fig. 8(a) shows the effect of a thick wall, i.e. Model A on volumetric change during diastole compared with that of model C and exact values. Since outer size of ventricles are similar for the shown cases, thickening if an inner wall in model A amounts to lowering the initial volume as can be seen in Fig. 8(a). However, this initial volume difference does not remain constant and increases at later times. The shape difference between real (healthy) and diseased heart will be discussed in later sections.

Since the CT scan images used in Kheirandish's [48] studies are the same as those used in the current study, it is of interest to compare the current results with those of [48]. Fig. 8(c) shows that the Kheirandish's results deviate to some extent from experimental data, however, model C results again produces a closer match of real results. Other than different initial volumes of model C and that of [48], the main difference between these two works is the application of inlet velocity boundary condition in [48] and pressure boundary condition in the present study. Kheirandish assumed unsteady physiological velocity at the inlet, i.e. mitral valve, while in current work, the physiological pressure is defined at the inlet surface. Although, Kheirandish's results for left ventricular volume change are relatively different from correct values, but the computed shape and deformations are not also accurate and even non-comparable with CT scan images.

Fig. 9 shows the deformation predicted by [48] which is quite abnormal as can be clearly seen. It should be noted that the inlet velocity BC, used in [48] dictates the left ventricular volume change to the fluid domain, since the fluid volume entering the left ventricle at each time is equal to the surface integral of fluid velocity at the fixed area inlet of left ventricle. The comparison between the erroneous shapes of Kheirandish work (Fig. 9) and shape changes of the current study during diastole will be discussed later in Fig. 18 that proves the importance of choosing an appropriate inlet boundary condition which is the inlet physiological pressure shown in Fig. 4.

Fig. 10 demonstrates the change of average ventricular pressure for three models with physiological average left ventricular pressure, extracted from Guyton and Hall's medical physiology textbook [53]. Although for validation purpose, the numerical results should be compared with the experimental data of the specific person which will be presented in later sections, but the trend of average left ventricular pressure change for numerical and experimental data can be studied and discussed. According to Fig. 10, the trends of pressure change during diastole for models B and C are similar to physiological chart, but at the beginning of diastole the results of these models are far from physiological data. The physiological mean pressure chart descends drastically from a peak in a very short interval at the beginning of diastole. This significant decrease is due to the cyclic contraction and expansion of the heart muscle which is intrinsically an effect of electrical waves on the heart tissue. At the beginning of diastole, the electric waves guided inside the heart tissue, induce the isovolumetric relaxation step. At isovolumeric relaxation, the ventricle loosens and the ventricular pressure decreases rapidly. Since in the current study the electrical interactions are not taken to account, therefore the differences between results of Fig. 10 at the beginning of diastole is logical. It should be noted that all present fluid-solid simulations during diastole are started and continued by applying the atrial pressure shown in Fig. 4 and no electrical wave travel in hearth tissues is considered. Therefore, it can be expressed that early filling phase at the start of diastole is not correctly modeled.

For model C, from time 0.09s to 0.3s the numerical curve has a good accordance with experimental data. The difference in the mean ventricular pressures of models B and C can be justified as the absence of pressure loss from atrium inlet to ventricular inlet in model B. Therefore, with the same pressure boundary condition at the inlets of both models, the ventricular pressure of model C is less than that of model B. In the time interval from 0.38s to 0.5s, i.e. the atrium systole, the physiological data has a peak in mean pressure, which is captured by both models B and C. Also the pressure predicted by model A with thickened wall is much more than the others which is expectable.

2-1-2 Velocity contours and streamlines in the left ventricle

In this section, the fluid velocity fields along with streamlines projected on different planes are presented. Fig. 11 shows two assumed plane sections.

As shown in Fig. 12, at the beginning of heart cycle, at time 0.04s, flow with large velocity magnitude enters left ventricle from mitral valve and augments the ventricular volume. But at the beginning of diastole, around 0.04s, for model B without atrium, the velocity magnitude from mitral valve entering left ventricle is greater than that of model C. Also at the time 0.15s for both models, it is observed that the velocity decreases at the outlet of mitral valve, due to decrease of pressure at the inlet of mitral valve. As time passes, the velocity increases at the outlet of mitral

valve and at time 0.45s, velocity reaches its maximum. Besides, it can be perceived for all times, the maximum of velocity for model C is less than that of model B, which is justified as a result of pressure losses in the atrium of model B and the same boundary conditions at inlets of both models. According to Fig. 12, the maximum of velocity at the outlet of mitral valve for models B and C are respectively 1.876m/s and 1.772m/s.

The two-dimensional projected streamlines on planes 1 and 2 are presented in Fig. 13 at various times. According to Fig. 13, at time 0.04s, a small vortex is generated in both models B and C that becomes bigger and stronger in later times. However, the position and strength of these vortices are different in models B and C, especially at time 0.45s. At this time, the vortex in model C leans more toward the left wall of ventricle. The vortex position in model B at time 0.45s is closer to the middle of ventricle that affects loading and deformation of walls. Another smaller vortex is present in model B, close to aortic valve at times of 0.25s and 0.45s that is absent in model C. These differences can be attributed to the presence of atrium in model C that affects the exiting streamlines from the mitral valve, Fig. 12 at times 0.25s and 0.45s. Due to these different flow structures of models B and C, various shapes of left ventricle and deformations can be inferred in Fig. 13.

To investigate further the unsteady vortices initiation and flow forming, the three-dimensional path-lines can also be studied. The three-dimensional path-lines are assumed to be started from the mitral valve and propagate in the left ventricle. Fig. 14 shows the path-lines history for model B. Time variation of path-lines colored by velocity magnitude show the maximum velocity occurs at time 0.45s. This variation generates the flow field vortices of Fig. 13.

2-2 Solid domain

2-2-1 Deformation results

In this section, the results of deformation of mitral valve for models B and C are presented. According to Fig. 15, mitral valve deformation during time is similar for both models B and C, but the magnitude of deformation of mitral valve, hence amount of valve opening for model B is greater than model C for all times. The maximum deformation of mitral valve for models B and C are approximately 12mm and 11mm and the main point for larger deformation of model B is the higher pressure on the mitral valve caused by the absence of atrium in model B. This larger opening of Model B, is one of the reasons behind larger volume change in Fig. 8b and higher velocities of model B in Fig. 12.

Fig. 16 illustrates the deformation contours drawn on a cross sectional surface of left ventricle and mitral valve for both models B and C. The maximum deformation is 20.4 mm for model B and 15.6mm for model C. The maximum deformation of ventricular wall occurred at the lower part of the heart, as a vertical displacement of apex caused by fixation of the upper inlets and ventricle

volume change for each model. This is also in accordance with larger volume change of model B compared to model C, Fig. 8b and hence larger ventricular pressure of model B in Fig. 10 .

2-2-2 Comparison of numerical results with CT scan images

To evaluate the computational results, the results of model B are compared with CT scan images. The CT images used to extract the initial geometry of the simulations and at later times simulation results of ventricle shape are compared with CT scan images in 21 phases. The time period for taking each CT image is 0.0385s. Taking the total heart cycle as 0.8s which covers these 21 CT phases, 13 phases are related to diastole and the other 8 phases are related to systole. The beginning of diastole in the mentioned CT scan images, is from phase 35% in which the left ventricle has its minimum volume up to phase 95% at the of diastole. Table 3 shows the time interval of diastole phases, considering the time interval for photographing each phase is 0.0385s.

To compare the left ventricle geometry of CT scan images with that of model B, four phases are chosen arbitrarily among the 13 mentioned phases. The numerical results of model B are extracted at the mean time of each CT scan phase. The cross sectional plane cut of the numerical results is exactly identical with cross section surface used for CT scan image shown in Fig. 17.

Fig. 18 shows the comparison between the shapes of model B and CT scan images for the ventricular wall at different time steps. The accordance of two shapes are remarkable at all times. Especially if we consider the abnormal deformation of the heart model shown in Fig. 9 obtained with inlet velocity BC, [48], the above agreement is highlighted. Therefore, it can be concluded that not only, the calculated ventricular volume changes for model B and those extracted from CT images are in good agreement, but also, the shapes of model B and CT scan images are quite close. This is true only if the pressure BC is used for the computations instead of velocity BC.

Conclusion

Having a complete heart model is imperative for exact performance prediction, however the computational burden is prohibitive. Therefore, a correct and less complex model of the heart is demanding. Value of a correct FSI simulation tool for heart modeling can be appreciated through the comparison of results with real life data images in the present study. More exact heart model and performance may be obtained through considering different parts such as atrium or mitral valve and choosing and tuning different numerical details such as BC’s., sufficiently complex models could be used for various purposes. In order to achieve a more precise model for heart simulation this study has been taken.

It is shown that the pressure BC instead of velocity BC at the inlet surface of left ventricle, i.e. the mitral valve, leads to better computational results for the solid domain deformation (shapes and volume change) compared with CT scan images.

Using real CT scan images, three different models are constructed: Model A comprising of the left ventricle and mitral valve with intentionally thickened ventricular wall as a simple model of Left Ventricular Hypertrophy (LVH), Model B involving left ventricle with mitral valve and model C including left ventricle, mitral valve and atrium. Model A is taken only as an example of changing the geometry due to a disease and the resulting outcome of FSI simulation, showing noticeable decrease in volume change and obvious increase of average ventricular pressure of LVH with respect to other models. Consequently, Left ventricular ejection fraction decreases.

To investigate the accuracy of results, ventricular volume change during diastole for three models are compared with physiological and experimental values extracted from CT images. The mean error, as the relative difference of volume change, between different models and experiments are 6% and 1.25%, for models B and C, respectively. It can be concluded that the mean and maximum error of model C which has the most realistic and complete geometry is considerably lower than models B.

The average ventricular pressure for model C is less than of model B which can be justified as a result of pressure loss from atrium inlets to mitral valve in the model C. For the same reason, the maximum velocity at the mitral valve outlet is always greater for model B than model C during the diastole. Additionally, the specific shape of atrium which is present in model C, directly affects the entrance flow to the mitral valve, hence the deformation of mitral valve.

To validate the results of solid domain, computed shapes of ventricular wall are compared with CT scan images. It is observed that shapes and deformations of ventricular wall are in good agreement with CT scan images. This is in contrast to previous simulations using inlet velocity BC, [49]. Although mitral valve deformations are the same for both models B and C, but for whole diastole, the amount of valve opening for model B is greater than model C. The maximum deformation of ventricular wall occurs at apex of left ventricle of model B which is bigger than model C due to larger volume change of model B.

Considering the above mentioned results, it can be concluded that for an accurate simulation of heart performance, it is essential to construct a model as close and as complete to real geometry as possible and as related. Clearly, FSI simulation may lead to feasible results only when relevant numerical details such as usage of inlet pressure condition is exercised. More complete heart geometry and considering multi-physics phenomena such heart electrical subsystem may eventually provide the necessary numerical tool for practical applications. Also, in future the comparison of the FSI simulation details with the results of cardiovascular magnetic resonance (CMR) imaging [53] would provide deeper and through understanding of physical behavior of the hearth functioning.

Acknowledgement

The authors would like to thank Mr. Kheirandish who provided the CT scan images which he had previously captured and used in his own study.

References

[1] World Health Organization, "Cardiovascular Diseases," https://www.who.int/news-room/fact-sheets/detail/cardiovascular-diseases

[2] Badano, L.P., Kolias, T.J., Muraru, D., et al. "Standardization of left atrial, right ventricular, and right atrial deformation ….", *European Heart Journal-Cardiovascular Imaging*, **19**(6), pp.591-600, (2018). https://doi.org/10.1093/ehjci/jey042

[3] Lange, T. and Schuster, A., "Quantification of myocardial deformation applying CMR-feature-tracking—All about the left ventricle? " *Current Heart Failure Reports*, **18**, pp.225-239, (2021).

[4] Peirlinck, M., Sahli Costabal, F., Yao, J., et al. "Precision medicine in human heart modeling: Perspectives, challenges, and opportunities." *Biomechanics and Modeling in Mechanobiology*, **20**, pp.803-831, (2021). https://doi.org/10.1007/s10237-021-01421-z

[5] Quarteroni, A. and Fedele, M. "Polygonal surface processing and mesh generation tools for the numerical simulation of the cardiac function." *International journal for numerical methods in biomedical engineering*, **37**(4), pp.e3435, (2021). https://doi.org/10.1002/cnm.3435

[6] Wang, D., Qian, Z., Vukicevic, M., et al. "3D printing, computational modeling, and artificial intelligence for structural heart disease." *Cardiovascular Imaging*, **14**(1), pp.41-60, (2021). https://doi.org/10.1016/j.jcmg.2019.12.022

[7] Garber, L., Khodaei, S. and Keshavarz Motamed, Z. "The critical role of lumped parameter models in patient-specific cardiovascular simulations." *Archives of Computational Methods in Engineering*, **29**(5), pp.2977-3000, (2022). https://doi.org/10.1007/s11831-021-09685-5

[8] Fang, Y., Sun, W., Zhang, T., et al. "Recent advances on bioengineering approaches for fabrication of functional engineered cardiac pumps: A review." *Biomaterials*, **280** pp.121298, (2022). https://doi.org/10.1016/j.biomaterials.2021.121298

[9] Yadid, M., Oved, H., Silberman, E., et al. "Bioengineering approaches to treat the failing heart: from cell biology to 3D printing." *Nature Reviews Cardiology*, **19**(2), pp.83-99, (2022). https://doi.org/10.1016/j.biomaterials.2021.121298

[10] Fedele, M., Piersanti, R., Regazzoni, F., et al. "A comprehensive and biophysically detailed computational model of the whole human heart electromechanics." *Computer Methods in Applied Mechanics and Engineering*, **410**, pp.115983, (2023). https://doi.org/10.1016/j.cma.2023.115983

[11] Peskin, C. S., "The immersed boundary method," *Acta numerica*, **11**, pp. 479-517, (2002). https://doi.org/10.1017/S0962492902000077

[12] Yoganathan, A. P., Lemmon Jr, J. D., Kim, Y.H., et al. "A computational study of a thin-walled three-dimensional…" *Journal of biomechanical engineering*, **116**(3), pp. 307-314, (1994). https://doi.org/10.1115/1.2895735

[13] Lemmon, J. and Yoganathan, A., "Computational modeling of left heart diastolic function: examination of ventricular dysfunction," *Journal of biomechanical engineering*, **122**(4), pp. 297-303, (2000). https://doi.org/10.1115/1.1286559

[14] Zheng, X., Seo, J. H., Vedula, V., et al. "Computational modeling and analysis of intracardiac flows in simple models of the left ventricle," *European Journal of Mechanics-B/Fluids*, **35**, pp. 31-39, (2012). https://doi.org/10.1016/j.euromechflu.2012.03.002

[15] Nakamura, M., Wada, S., Mikami, T., et al. "A computational fluid mechanical study on the effects of opening and closing of the mitral orifice …" *JSME International Journal Series C Mechanical Systems, Machine Elements and Manufacturing*, **45**(4), pp. 913-922, (2002). https://doi.org/10.1299/jsmec.45.913

[16] McQueen, D. and Peskin, C., "A three-dimensional computer model of the human heart for studying cardiac fluid dynamics," *ACM SIGGRAPH Computer Graphics*, **34**(1), pp. 56-60, (2000). https://doi.org/10.1145/563788.604453

[17] Vierendeels, J. A., Riemslagh, K., Dick, E., et al. "Computer simulation of intraventricular flow and pressure gradients during diastole," *Journal of Biomechanical Engineering*, **122**(6), pp. 667-674, (2000). https://doi.org/10.1115/1.1318941

[18] Watanabe, H., Sugiura, S., Kafuku, H., et al. "Multiphysics simulation of left ventricular filling dynamics using fluid-structure interaction finite element method," *Biophysical journal*, **87**(3), pp. 2074-2085, (2004). doi: 10.1529/biophysj.103.035840

[19] Cheng, Y., Oertel, H. and Schenkel, T., "Fluid-structure coupled CFD simulation of the left ventricular flow during filling phase," *Annals of biomedical engineering*, **33**(5), pp. 567-576, (2005). https://doi.org/10.1007/s10439-005-4388-9

[20] Lau, K. D., Diaz, V., Scambler, P., et al. "Mitral valve dynamics in structural and fluid–structure interaction models," *Medical engineering & physics*, **32**(9), pp. 1057-1064, (2010). https://doi.org/10.1016/j.medengphy.2010.07.008

[21] Dahl, S. K., Vierendeels, J., Degroote, J., et al. "FSI simulation of asymmetric mitral valve dynamics during diastolic filling," *Computer methods in biomechanics and biomedical engineering*, **15**(2) , pp. 121-130, (2012). https://doi.org/10.1080/10255842.2010.517200

[22] Arefin, M. and Morsi, Y., "Fluid structure interaction (FSI) simulation of the left ventricle (LV) during the early filling wave (E-wave), diastasis and atrial contraction wave (A-wave)," *Australasian physical & engineering sciences in medicine*, **37**(2), pp. 413-423, (2014). https://doi.org/10.1007/s13246-014-0250-4

[23] Su, B., Zhong, L., Wang, X. K., et al. "Numerical simulation of patient-specific left ventricular model with both mitral and aortic valves by FSI approach," *Computer methods and programs in biomedicine*, **113**(2), pp. 474-482, (2014). https://doi.org/10.1016/j.cmpb.2013.11.009

[24] Arefin, M., "An investigation on the effects of the angles between the mitral and aortic orifice during diastolic period using FSI," *Pathophysiology*, **24**(3), pp. 133-153, (2017). https://doi.org/10.1016/j.pathophys.2017.03.002

[25] Nakamura, M., Wada, S., Mikami, T., et al. "Computational study on the evolution of an intraventricular vortical flow during early diastole for the interpretation of color M-mode Doppler echocardiograms," *Biomechanics and modeling in mechanobiology*, **2**(2), pp. 59-72, (2003). https://doi.org/10.1007/s10237-003-0028-1

[26] Tang, D., Yang, C., Geva, T., et al. "Image-based patient-specific ventricle models with fluid–structure interaction for cardiac function assessment and surgical design optimization," *Progress in Pediatric Cardiology*, **30**(1-2), pp. 51-62, (2010). https://doi.org/10.1016/j.ppedcard.2010.09.007

[27] Taylor, T. and Yamaguchi, T., "Realistic three-dimensional left ventricular ejection determined from computational fluid dynamics," *Medical engineering & physics*, **17**(8), pp. 602-608, (1995). https://doi.org/10.1016/1350-4533(95)00017-H

[28] Su, B., Tan, R. S., Tan, J. L., et al. "Cardiac MRI based numerical modeling of left ventricular fluid dynamics with mitral valve incorporated," *Journal of biomechanics*, **49**(7), pp. 1199-1205, (2016). https://doi.org/10.1016/j.jbiomech.2016.03.008

[29] Su, B., Zhang, J. M., Tang, H. C., et al. "Patient-specific blood flows and vortex formations in patients with hypertrophic cardiomyopathy using computational fluid dynamics," *2014 IEEE Conference on Biomedical Engineering and Sciences (IECBES)*, pp. 276-280, (2014). doi: 10.1109/IECBES.2014.7047502

[30] Saber, N., Gosman, R. A. D., Wood, N. B., et al. "Computational flow modeling of the left ventricle based on in vivo MRI data: initial experience," *Annals of biomedical engineering*, **29**(4), pp. 275-283, (2001). https://doi.org/10.1114/1.1359452

[31] Ebbers, T., Wigstro, L., Bolger, A. F., et al. "Noninvasive measurement of time-varying three-dimensional relative pressure fields within the human heart," *Journal of biomechanical engineering*, **124**(3), pp. 288-293, (2002). https://doi.org/10.1115/1.1468866

[32] Long, Q., Merrifield, R., Xu, X. Y., et al. "Intra-ventricular blood flow simulation with patient specific geometry," *In 4th International IEEE EMBS Special Topic Conference on Information Technology Applications in Biomedicine*, pp. 126-129, (2003). doi: 10.1109/ITAB.2003.1222489

[33] Long, Q., Merrifield, R., Xu, X. Y., et al. "Subject-specific computational simulation of left ventricular flow based on magnetic resonance imaging," *Proceedings of the Institution of Mechanical Engineers, Part H: Journal of Engineering in Medicine*, **222**(4), pp. 475-485, (2008). doi.org/10.1243/09544119jeim310

[34] Doenst, T., Spiegel, K., Reik, M., et al. "Fluid-dynamic modeling of the human left ventricle: methodology and application to surgical ventricular reconstruction," *The Annals of thoracic surgery*, **87**(4), pp. 1187-1195, (2009). https://doi.org/10.1016/j.athoracsur.2009.01.036

[35] Khalafvand, S. S., Yin-Kwee Ng, E., Zhong, L., et al. "Fluid-dynamics modelling of the human left ventricle with dynamic mesh for normal and myocardial infarction: preliminary study," *Computers in biology and medicine*, **42**(8), pp. 863-870, (2012). https://doi.org/10.1016/j.compbiomed.2012.06.010

[36] Chen, L., Liu, J., Hong, H., et al. "Medical image-based analysis of flow in heart with congenital heart disease: Numerical simulation of intraventricular flow," *In 2015 10th Asian Control Conference (ASCC)*, pp. 1-6, (2015). doi: 10.1109/ASCC.2015.7244764

[37] Chnafa, C., Mendez, S. and Nicoud, F., "Image-based large-eddy simulation in a realistic left heart," *Computers & Fluids*, **94**, pp. 173-187, (2014). https://doi.org/10.1016/j.compfluid.2014.01.030

[38] Kerckhoffs, R. C., Faris, O. P., Bovendeerd, P. H., et al. "Timing of depolarization and contraction in the paced canine left ventricle: model and experiment," *Journal of cardiovascular electrophysiology*, **14**, pp. S188-S195, (2003). https://doi.org/10.1046/j.1540.8167.90310.x

[39] Sermesant, M., Moireau, P., Camara, O., et al. "Cardiac function estimation from MRI using a heart model and data assimilation: advances and difficulties," *Medical Image Analysis*, **10**(4), pp. 642-656, (2006). https://doi.org/10.1016/j.media.2006.04.002

[40] Keldermann, R., Nash, M., Gelderblom, H., et al. "Electromechanical wavebreak in a model of the human left ventricle," *American Journal of Physiology-Heart and Circulatory Physiology*, **299**(1), pp. H134-H143, (2010). https://doi.org/10.1152/ajpheart.00862.2009

[41] Nordsletten, D., Niederer, S., Nash, M., et al. "Coupling multi-physics models to cardiac mechanics," *Progress in biophysics and molecular biology*, **104**(1-3), pp. 77-88, (2011). https://doi.org/10.1016/j.pbiomolbio.2009.11.001

[42] Gurev, V., Lee, T., Constantino, J., et al. "Models of cardiac electromechanics based on individual hearts imaging data," *Biomechanics and modeling in mechanobiology*, **10**(3), pp. 295-306, (2011). https://doi.org/10.1007/s10237-010-0235-5

[43] Pourmand, D. R., "Simulation of beating heart considering fluid solid interface," Shiraz University, Mechanical Engineering Department, (2012).

[44] Nordsletten, D., McCormick, M., Kilner, P., et al. "Fluid–solid coupling for the investigation of diastolic and systolic human left ventricular function," *International Journal for Numerical Methods in Biomedical Engineering*, **27**(7), pp. 1017-1039, (2011). https://doi.org/10.1002/cnm.1405

[45] Gao, H., Ma, X., Qi, N., et al. "A finite strain nonlinear human mitral valve model with fluid-structure interaction," *International journal for numerical methods in biomedical engineering*, **30**(12), pp. 1597-1613, (2014). https://doi.org/10.1002/cnm.2691

[46] Toma, M., Jensen, M., Einstein, D., et al. "Fluid–structure interaction analysis of papillary muscle forces using a comprehensive mitral valve model with 3D chordal structure," *Annals of biomedical engineering*, **44**(4), pp. 942-953, (2016). https://doi.org/10.1007/s10439-015-1385-5

[47] Seo, J., Vedula, V., Abraham, T., et al. "Effect of the mitral valve on diastolic flow patterns," *Physics of fluids*, **26**(12), p. 121901, (2014). https://doi.org/10.1063/1.4904094

[48] Kheirandish, S., Alishahi, M. M. and Abuali, O., "Numerical modeling of blood flow in left ventricle considering mitral valve during diastole phase," ISME2015-10100951724, Tehran, Iran, (2015).

[49] Si, W., Liao, X., Qin, J., et al. "Computational Modeling of Fluid–Structure Interaction Between Blood Flow and Mitral Valve," in *Computational Biomechanics for Medicine, Springer*, pp. 31-41, (2019). https:/doi.org/10.1007/978-3-319-75589-2_4

[50] Monfared, M., Alishahi, M. M. and Alishahi, M., "Precise Fluid-Solid Simulation of Human Left Ventricle along with Aortic Valve during Systole," *WSEAS Transactions on Fluid Mechanics*, **17**, pp. 18-38, (2022). DOI: 10.37394/232013.2022.17.3

[51] Messerli, F., Ventura, H., Elizardi, D., et al. "Hypertension and sudden death: increased ventricular ectopic activity in left ventricular hypertrophy," *The American journal of medicine*, **77**(1), pp. 18-22, (1984). https://doi.org/10.1016/0002-9343(84)90430-3

[52] Devereux, R., Alonso, D., Lutas, E., et al. "Echocardiographic assessment of left ventricular hypertrophy: comparison to necropsy findings," *The American journal of cardiology*, **57**(6), pp. 450-458, (1986). https://doi.org/10.1016/0002-9149(86)90771-X

[53] Hall, J. E. and Hall, M. E., *Guyton and Hall textbook of medical physiology e-Book*. Elsevier Health Sciences, (2020).

[54] Xiaodan, Z., Tan, R. S., Garg, P., et al. "Impact of age, sex and ethnicity on intra-cardiac flow components and left ventricular kinetic energy derived from 4D flow CMR." *International journal of cardiology*, **336**, pp. 106-112, (2021). https://doi.org/10.1016/j.ijcard.2021.05.035

[55] Holzapfel, G. A., Gasser, T. C. and Ogden, R. W., "A new constitutive framework for arterial wall mechanics and a comparative study of material models, " *Journal of elasticity and the physical science of solids*, **61**(1), pp.1-48, (2000). https://doi.org/10.1023/A:1010835316564

Figure Captions:

Fig. 1 (a) Left ventricle with thick wall with mitral valve, model a, (b) real geometry of left ventricle with mitral valve, model b, (c) real geometry of left ventricle with mitral valve and real shaped atrium, model c

Fig. 2 (a) Dimensions of mitral valve leaflets from ct images, (b) vertical view of reconstructed mitral valve used in the present study, (c) top view of designed mitral valve

Fig. 3 Fluid boundary condition for three models (a), (b) and (c)

Fig. 4 Sixth order polynomial curve fit on the physiological left atrial pressure

Fig. 5 Solid boundary conditions for models (a), (b) and (c)

Fig. 6 Generated 3d grids and midsection cuts for (a) solid and (b) fluid domains

Fig. 7 Results of grid and time step independency study on the sample plane for fluid domain of model b

Fig. 8 Left ventricular volume change for (a) models a and c, along with ct scan data, (b) models b and c, with ct scan data, (c) model c, ct scan data, and previous numerical results of Kheirandish et al. [48]

Fig. 9 Contours of total deformation and the left ventricle shape during diastole using the inlet velocity boundary condition for fluid domain [48]

Fig. 10 Left ventricular average pressure change for models a, b and c along with physiological data

Fig. 11 Sectional planes for depicting velocity contours for model b (plane 1) and model c (plane 2)

Fig. 12 Velocity contours for models b (right) and c (left), drawn respectively on plane 1 and plane 2 at times 0.04s, 0.15s, 0.25s and 0.45s

Fig. 13 Two-dimensional streamlines for models b (right) and c (left), respectively projected on plane 1 and plane 2 at times 0.04s, 0.15s, 0.25s and 0.45s

Fig. 14 Three -dimensional path-lines inside the left ventricle for model b at the times 0.04s, 0.25s, 0.35s and 0.45s

Fig. 15 Contours of deformation for mitral valve for model c (left) and model b (right) at times 0.04s, 0.25s, 0.35s

Fig. 16 Contours of deformation for left ventricle and mitral valve for model b (right) and model c (left) at the times 0.04s, 0.25s, 0.35s and 0.45s

Fig. 17 The cutting plane used for comparing numerical results of model b with ct scan images data.

Fig. 18 Comparison between the shapes of model b and ct scan images for phases 35%, 65%, 85% and 95% at different times.

Table Titles:

Table 1. Coefficients of left arterial diastole pressure interpolation
($P = At^6 + Bt^5 + Ct^4 + Dt^3 + Et^2 + Ft + G$)

Table 2. Number of grids used in grid study analysis for each model

Table 3. The time interval of ct scan image phases during diastole

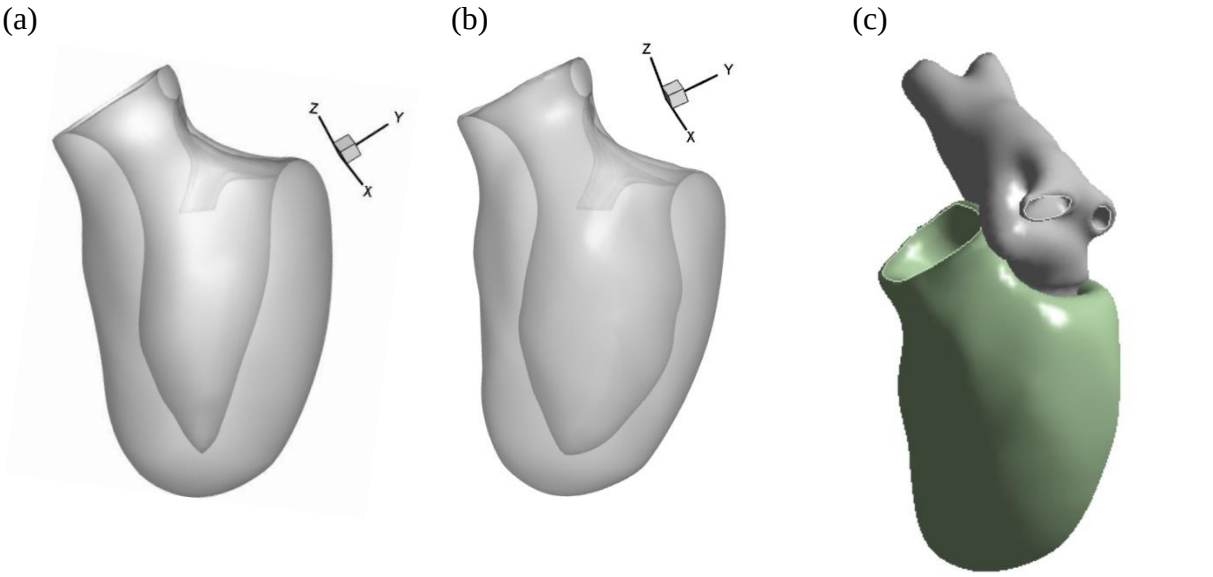

Fig. 1 (a) Left ventricle with thick wall with mitral valve, model a, (b) real geometry of left ventricle with mitral valve, model b, (c) real geometry of left ventricle with mitral valve and real shaped atrium, model c

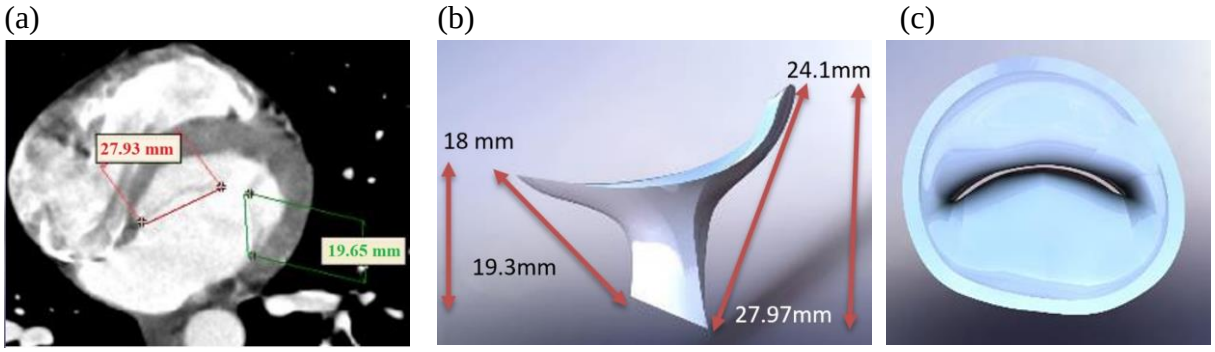

Fig. 2 (a) Dimensions of mitral valve leaflets from ct images, (b) vertical view of reconstructed mitral valve used in the present study, (c) top view of designed mitral valve

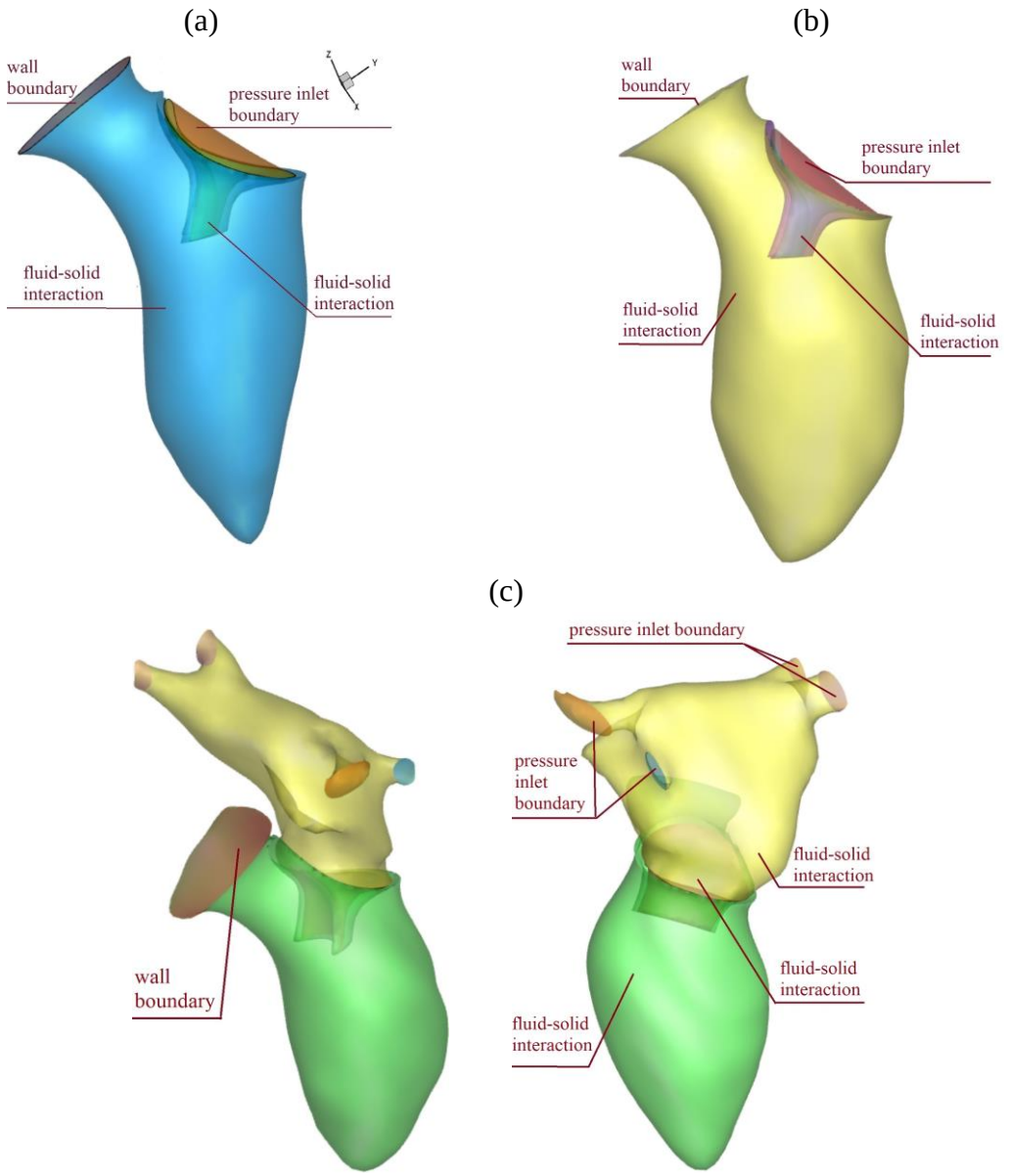

Fig. 3 Fluid boundary condition for three models (a), (b) and (c)

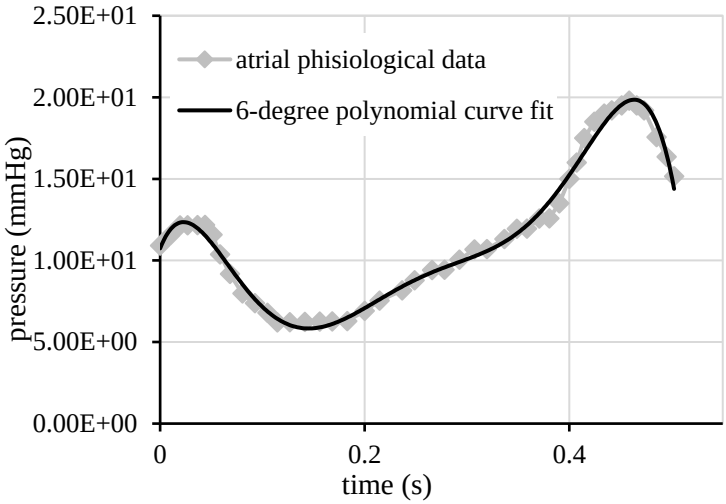

Fig. 4 Sixth order polynomial curve fit on the physiological left atrial pressure

(a)

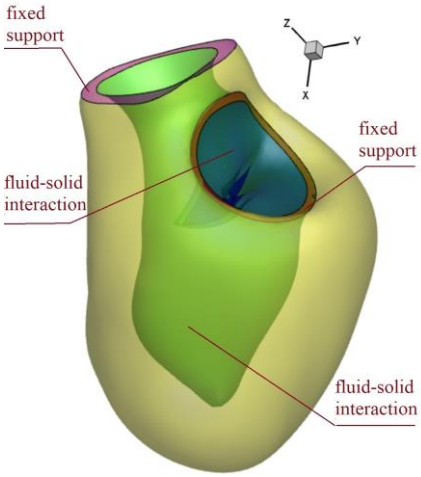

(b)

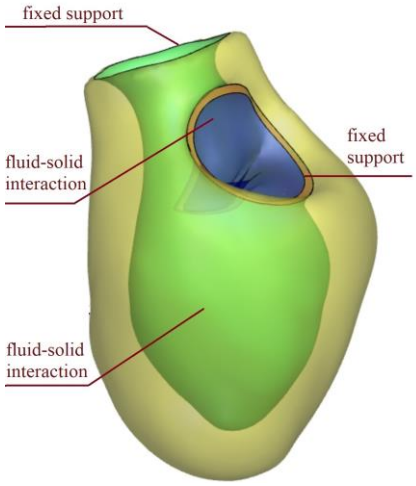

(c)

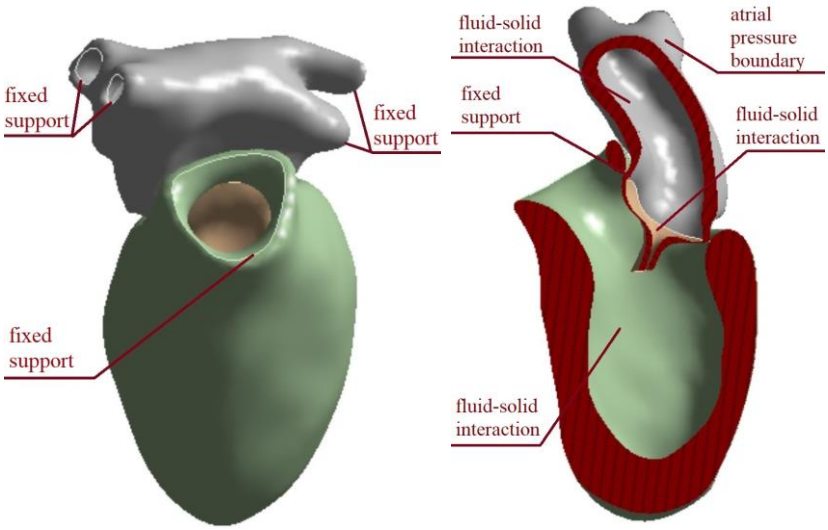

Fig. 5 Solid boundary conditions for models (a), (b) and (c)

(a) (b)

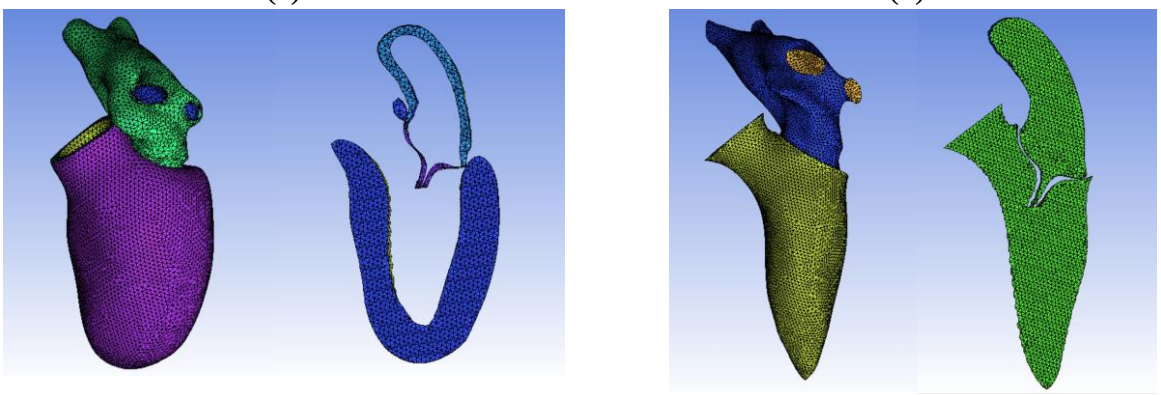

Fig. 6 Generated 3d grids and midsection cuts for (a) solid and (b) fluid domains

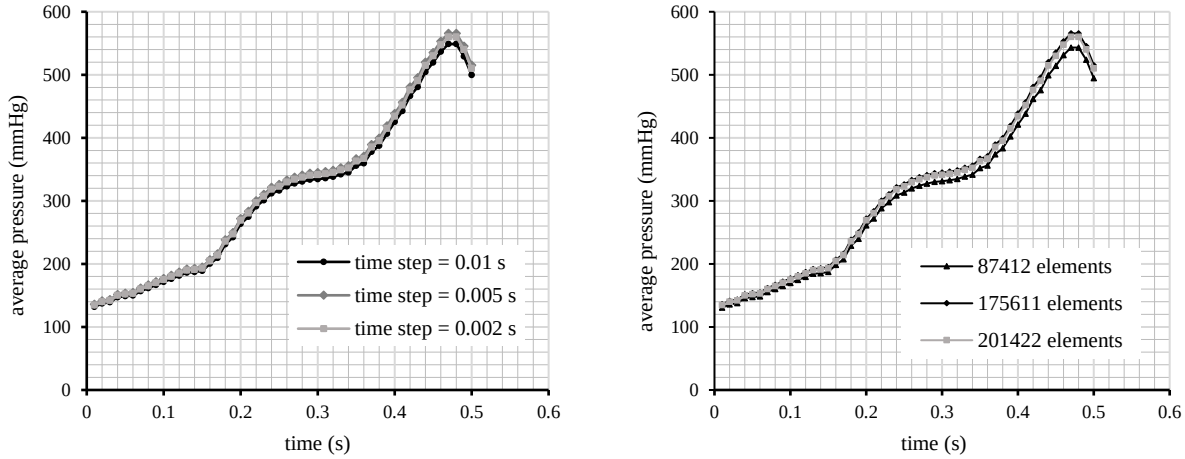

Fig. 7 Results of grid and time step independency study on the sample plane for fluid domain of model b

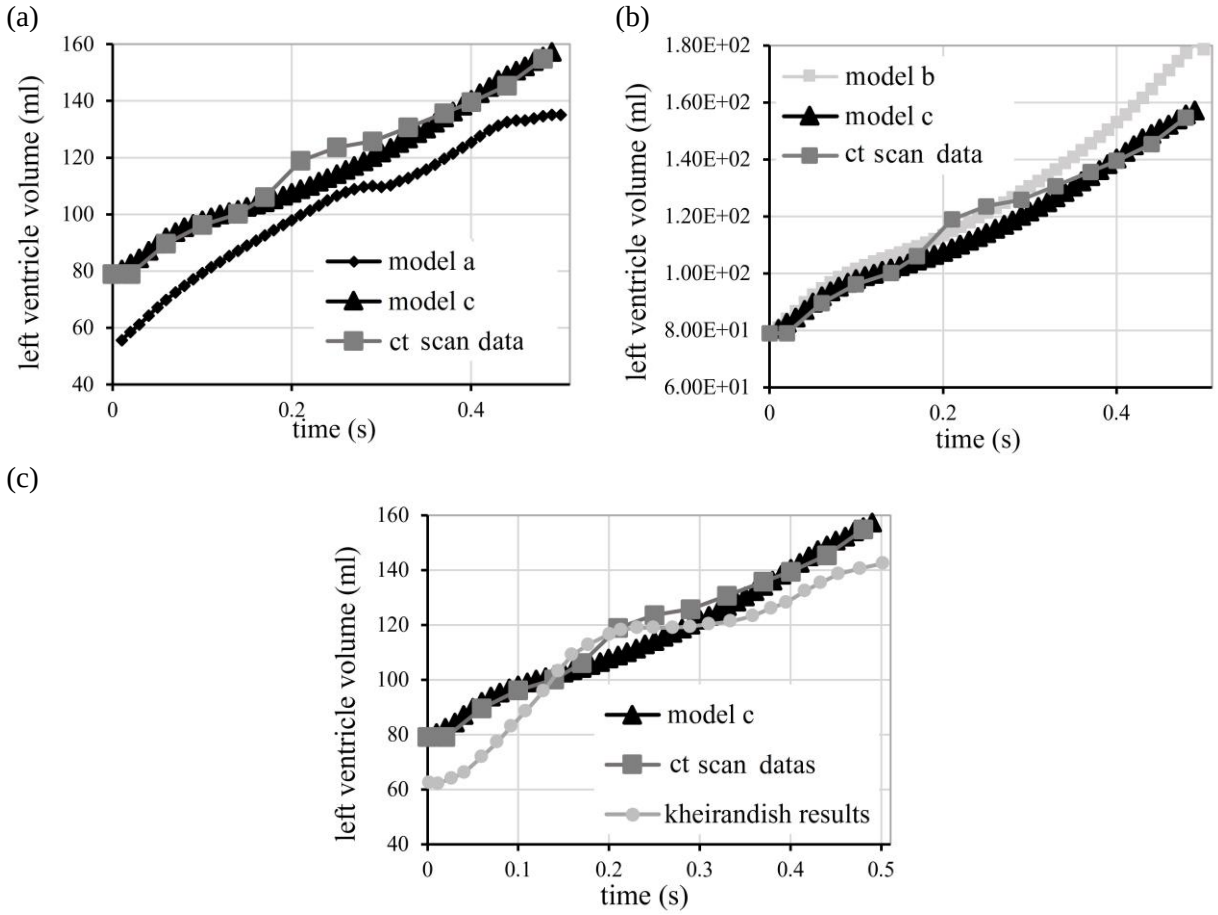

Fig. 8 Left ventricular volume change for (a) models a and c, along with ct scan data, (b) models b and c, with ct scan data, (c) model c, ct scan data, and previous numerical results of Kheirandish et al. [48]

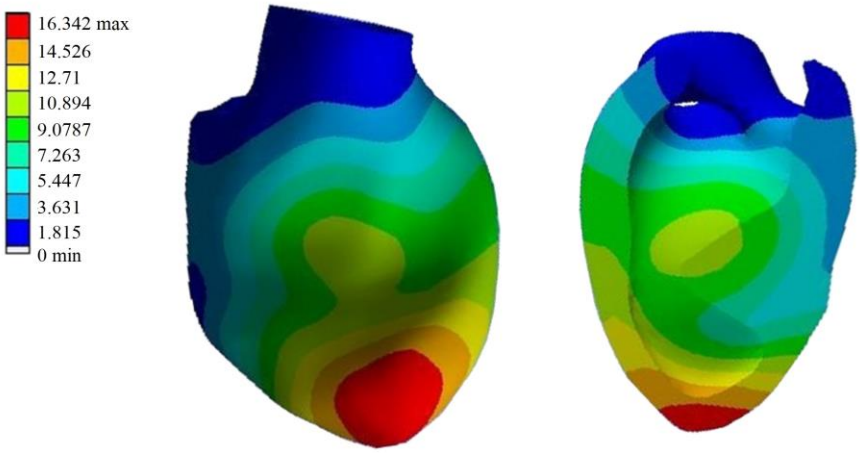

Fig. 9 Contours of total deformation and the left ventricle shape during diastole using the inlet velocity boundary condition for fluid domain [48]

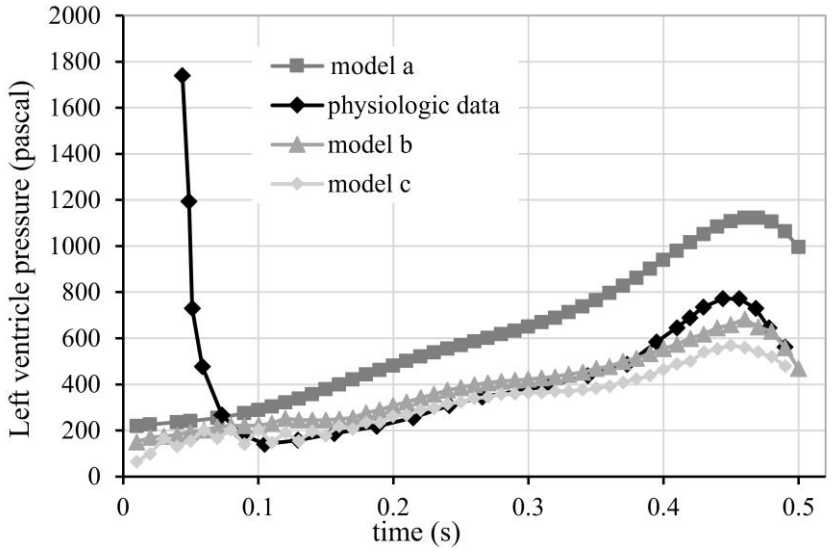

Fig. 10 Left ventricular average pressure change for models a, b and c along with physiological data

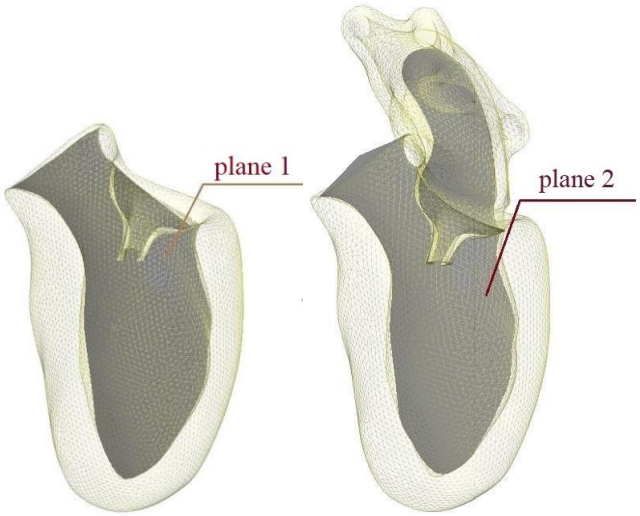

Fig. 11 Sectional planes for depicting velocity contours for model b (plane 1) and model c (plane 2)

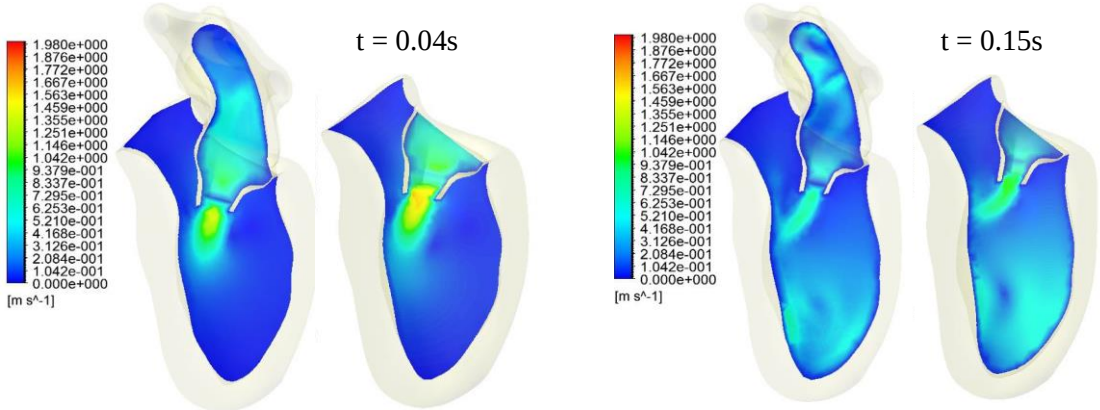

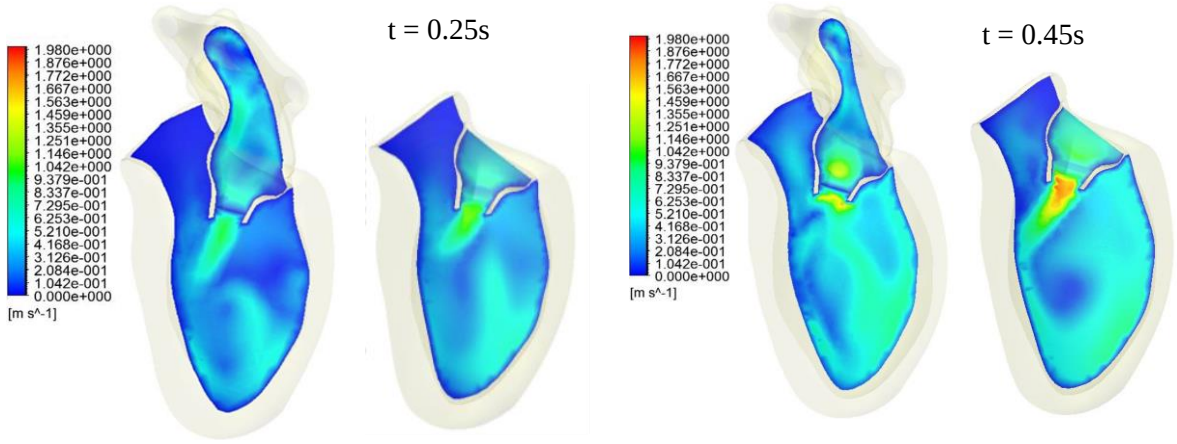

Fig. 12 Velocity contours for models b (right) and c (left), drawn respectively on plane 1 and plane 2 at times 0.04s, 0.15s, 0.25s and 0.45s

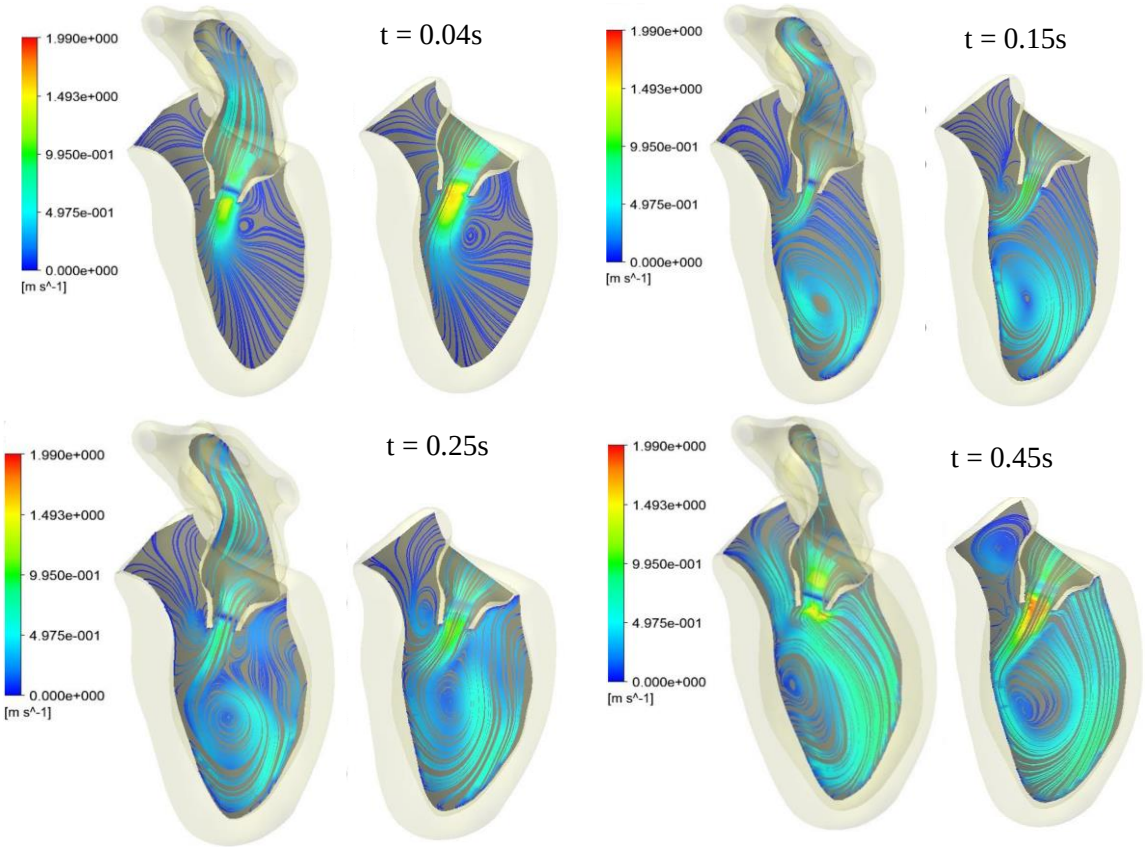

Fig. 13 Two-dimensional streamlines for models b (right) and c (left), respectively projected on plane 1 and plane 2 at times 0.04s, 0.15s, 0.25s and 0.45s

t = 0.04s t = 0.25s t = 0.35s t = 0.45s

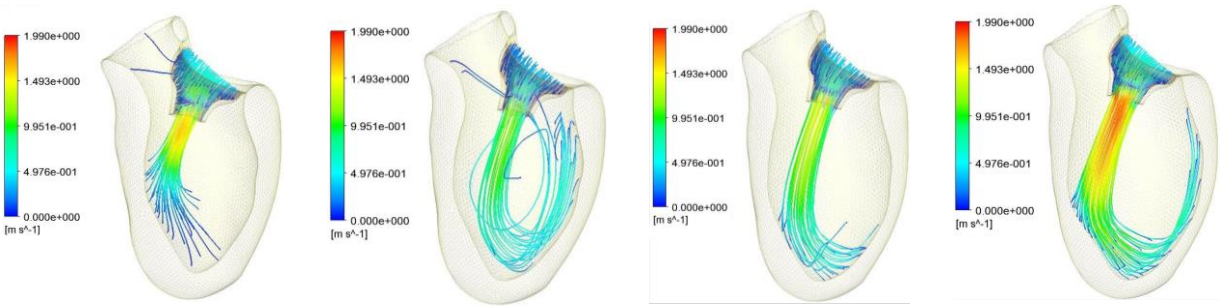

Fig. 14 Three -dimensional path-lines inside the left ventricle for model b at the times 0.04s, 0.25s, 0.35s and 0.45s

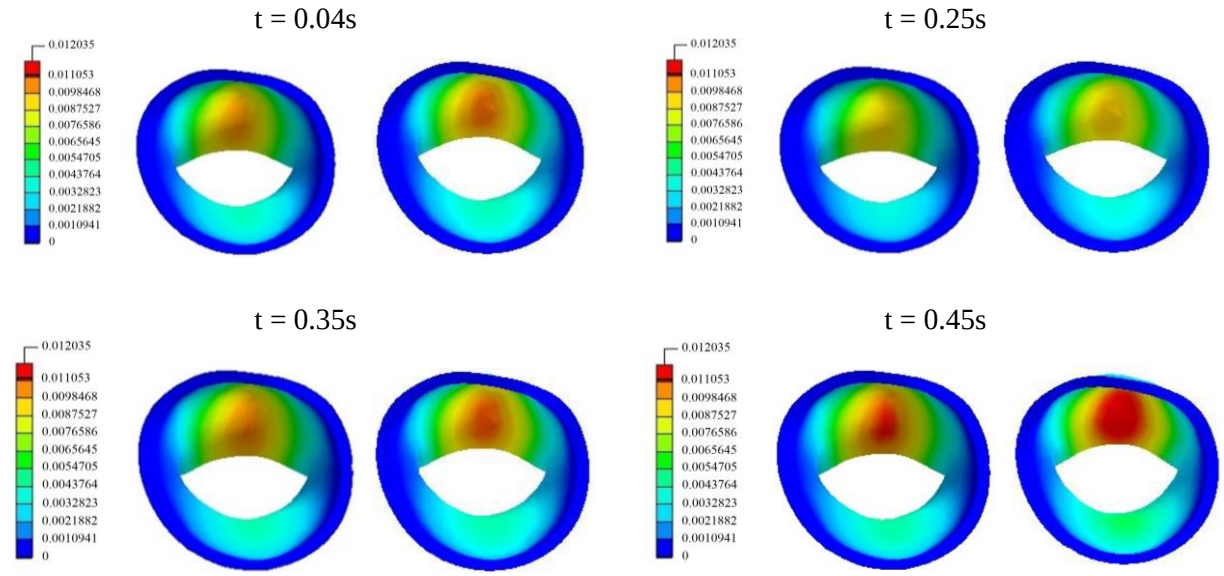

Fig. 15 Contours of deformation for mitral valve for model c (left) and model b (right) at times 0.04s, 0.25s, 0.35s and 0.45s

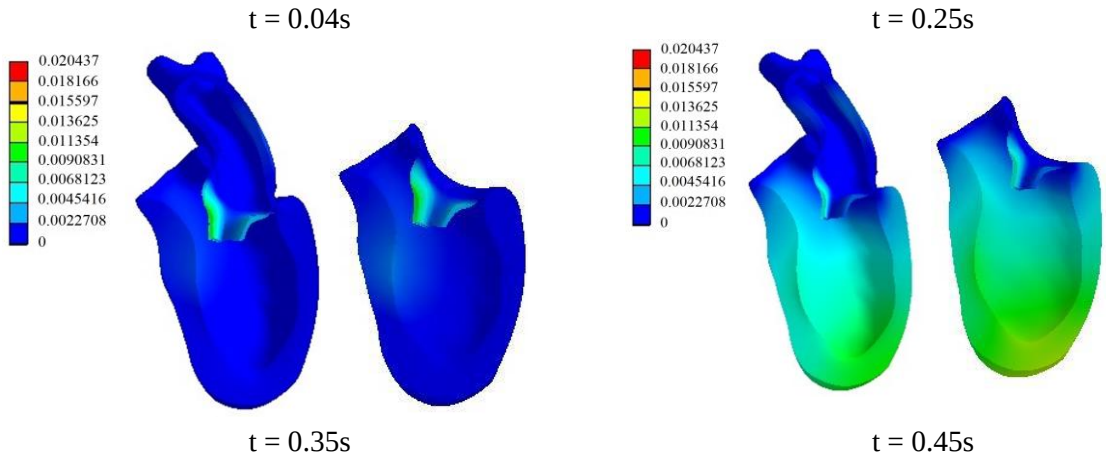

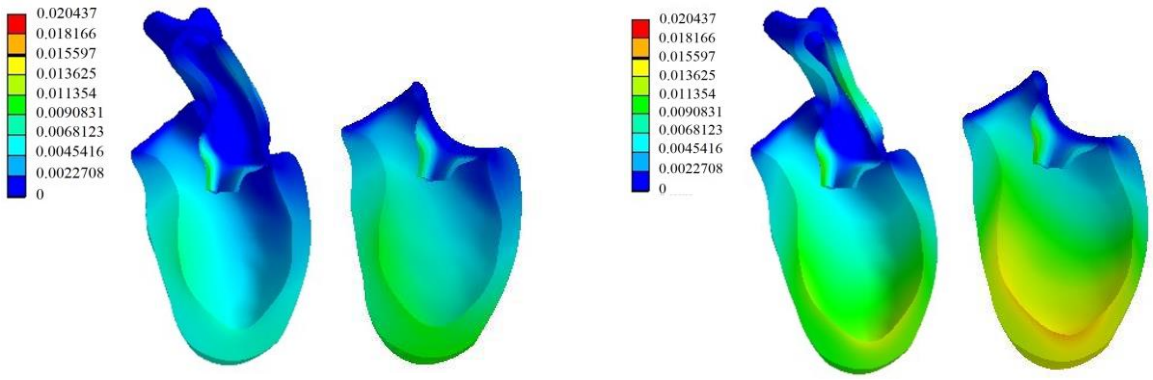

Fig. 16 Contours of deformation for left ventricle and mitral valve for model b (right) and model c (left) at the times 0.04s, 0.25s, 0.35s and 0.45s

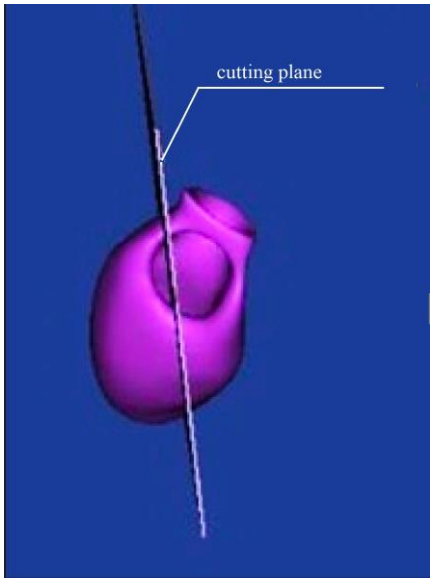

Fig. 17 The cutting plane used for comparing numerical results of model b with ct scan images data.

t_{avg} = 0.02s

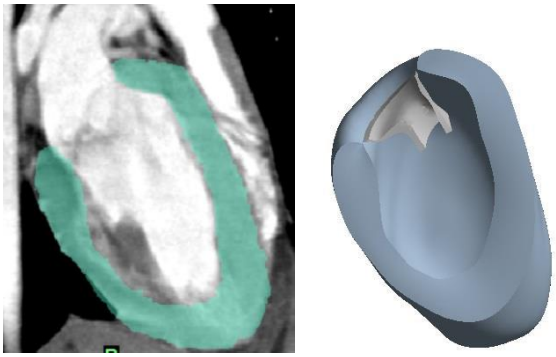

t_{avg} = 0.25s

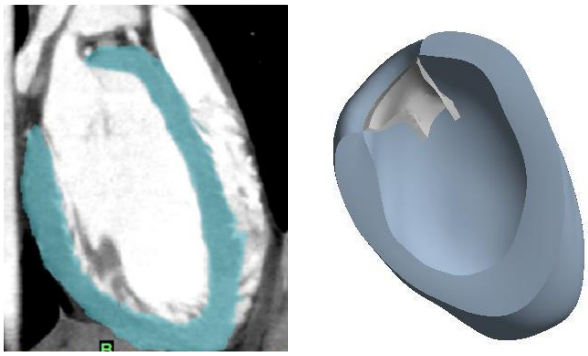

t_{avg} = 0.4s

t_{avg} = 0.48s

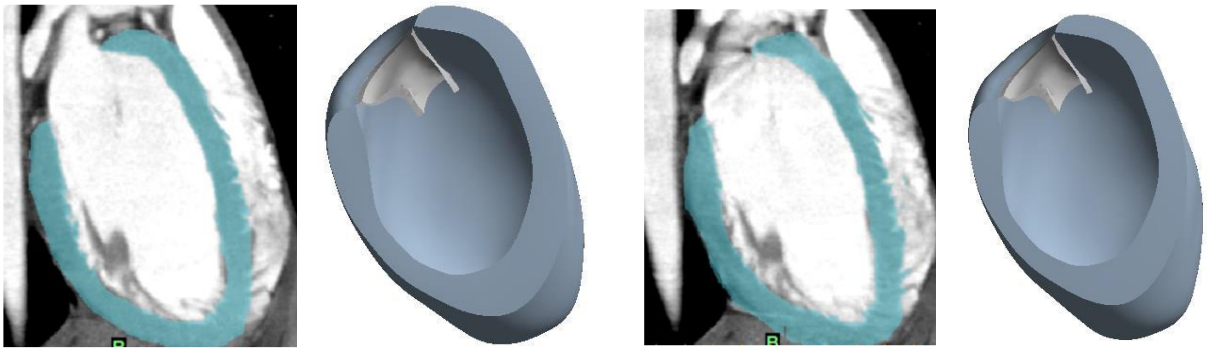

Fig. 18 Comparison between the shapes of model b and ct scan images for phases 35%, 65%, 85% and 95% at different times.

Table 1. Coefficients of left arterial diastole pressure interpolation

($P = At^6 + Bt^5 + Ct^4 + Dt^3 + Et^2 + Ft + G$)

$A = -197544$	$B = 288538$
$C = -159923$	$D = 41485$
$E = -4787.9$	$F = 161.07$
$G = 10.73$	

Table 2. Number of grids used in grid study analysis for each model

		model a	model b	model c
fluid domain	grid 1	76252	87412	98453
	grid 2	168427	175611	192846
	grid 3	200476	201422	220486
solid domain	grid 1	99512	102346	142357
	grid 2	139246	186453	208087
	grid 3	203274	246837	263197

Table 3. The time interval of ct scan image phases during diastole

phase percent (%)	time interval (s)	average time (s)
35	0 – 0.0385	0.02
40	0.0385 – 0.077	0.06
45	0.077 – 0.1155	0.1
50	0.1155 – 0.154	0.14
55	0.154 – 0.1925	0.17
60	0.1925 – 0.231	0.21
65	0.231 – 0.2695	0.25
70	0.2695 – 0.308	0.29
75	0.308 – 0.3465	0.33
80	0.3465 – 0.385	0.37

85	0.385 – 0.4235	0.4
90	0.4235 – 0.462	0.44
95	0.462 – 0.5	0.48

Arman Zohrabi is a Mechanical Engineering graduate from Shiraz University, specializing in fluid-structure interaction (FSI) simulations of blood flow in patient-specific models of the human left ventricle during diastole. His thesis also focused on analyzing the effects of mitral valve diseases on blood flow dynamics in the left ventricle. During these years, he has worked on various computational fluid dynamics (CFD) studies and contributed to a research project on large eddy simulation (LES) modeling of air flow over a backward-facing step.

Dr. Mohammad Mehdi Alishahi is a Professor of Mechanical Engineering at Shiraz University, since 1982. His area of expertise includes computational and experimental fluid dynamics and aerodynamics. His current interest covers complex fluid dynamics modeling and experimentation such as vortex bursting and stability of two phase flows. Presently, his experimental work is focused on transonic wind tunnel testing and aeroballistics experimentation of models.

Dr. Marzieh Alishahi completed her graduate studies in Mechanical Engineering at Shiraz University. Since then, she has been working on various numerical and experimental projects related to fluid mechanics. Her research focuses on non-Newtonian fluids, rheology, computational fluid dynamics (CFD), and experimental fluid measurements.